This article is published in Composite Structures Journal

Highlights

• Lateral Torsional Buckling of Pultruded Fibre Reinforced Polymer (PFRP) is studied through numerical analysis.

• A simplified numerical modeling method is suggested.

• The influence of vertical load height, initial out-of-straightness, and lateral load eccentricity was explored.

• The combined effect of imperfections and load eccentricity may decrease or increase the load up to 17% and 19%, respectively.

• A suggestion for the design of PFRP I beams is summarized.

Influence of Combined Imperfections on Lateral-torsional Buckling Behaviour of Pultruded FRP Beams

T.T. Nguyen[a], Sivaganesh Selvaraj[b], T.-M. Chan[1,b], J.T. Mottram[c]

[a]*Institute of Civil Engineering, Ho Chi Minh City University of Transport, Vietnam*

[b]*Department of Civil and Environmental Engineering, The Hong Kong Polytechnic University, Hong Kong*

[c]*School of Engineering, University of Warwick, United Kingdom*

ABSTRACT

By way of computational analyses using Finite Element (FE) software this paper presents, by way of sensitivity studies, lateral-torsional buckling resistances of I-beams made of pultruded fibre reinforced polymer. Parameters changed in the studies are the geometric imperfections, the vertical load position and the load eccentricity. Measured geometrical and material imperfections are incorporated into the geometrical nonlinear FE simulations. Constants in the FE work are three-point bending loading and the imperfection condition from having different elastic constants in the four flange outstands. Numerical results from the sensitivity studies are verified by comparing them with equivalent buckling load results from a series of physical tests conducted previously. It is found that the influence of combined geometrical and material imperfections on LTB failure can be significant, such that an imperfect beam can be put into a near 'perfect imperfection' condition, in which it possesses a higher buckling resistance. The opposite can happen for a 'more severe imperfection' with poorer beam response under loading. The load eccentricity on I-beams confirms a complex structural response. To be able to have a

---

[1] Corresponding author. Tel: +852 2766 6013
Email: tak-ming.chan@polyu.edu.hk (T.M.Chan)

recognized design procedure for pultruded I-beam members the influence of combined imperfections on lateral-torsional buckling resistance needs to be reliably quantified.

Keywords: *Material and geometric imperfections, loading eccentricity, Finite Element analysis, Pultruded fibre reinforced polymer, lateral-torsional buckling.*

1. Introduction

Pultruded Fibre Reinforced Polymer (PFRP) sections have been increasingly used as structural components and systems in civil engineering works owing to their distinct advantages, such as high strength-to-weight ratios, environmental durability, magnetic and electronic transparent, and more [1]. These sections comprise of thin-walled panels of laminate materials made by the composite material process of pultrusion. In terms of their shapes, they can mimic the cross-section shapes found in conventional steel structures. To increase further the interest in PFRP structural sections there is a need to understand their structural behaviour. PFRP sections are used as beam members with the preferable shape an I-section. This cross-section can either be a single I-section or a 'built-up' section formed from two-channel (back-to-back) sections.

Lateral-torsional buckling (LTB) is an ultimate mode of failure of I-shaped beams under flexural deformation and can occur when the member is slender. The existence of this elastic instability can significantly reduce a beam's resistance over failure with another mode of ultimate failure [2]. Moreover, the presence of inherent geometrical imperfections, material imperfections and loading eccentricities will change, and this change can be significant, the structural responses and resistances of these PFRP beam members [3-4].

Akin to any structural component of any construction material, PFRP shapes are manufactured with inherent imperfections. Of importance to this study are the imperfections present in PFRP sections that are linked to material (e.g., variation of elastic constants in panels) and

geometrical properties (e.g., for out-of-straightness). The form of imperfection from a varying distribution of material properties has not been studied before. For example, the flange outstands and web in a I-section do not necessarily possess the same elastic constants [5, 6]. From the PhD work of the first author [6] the difference has been measured to be up to 20% in the case of the tensile longitudinal modulus of elasticity, which has symbol E_L or E_1, where subscript 'L' or '1' is for the axis coinciding with centroid of the I-section. It is further observed that the longitudinal modulus of elasticity in the web can be significantly lower [6], and this is attributed to different proportions of the two fiber reinforcement types in the pultrusion process [7]. The web-flange junctions can also have different material properties, again, as these regions can be resin-rich or fiber-poor compared to flange outstands and web panels. Although this physical feature has been studied by other researchers [8-11], the effect of changes in elastic constants at the web-flange junctions is not considered herein because the focused is on the global response of beam members. The presence the four fillet radii at the web-flange junctions is however included in the section properties of the I-shaped cross-section.

Over the years, several studies have been carried out to understand the overall instability response of thin-walled PFRP members. These structural investigations have led to knowledge and understanding on; local buckling [12-15], modal-interaction buckling [16], sectional distortion [17] and lateral-torsional buckling [2, 3, 4, 18]. Such incremental studies focused on the individual influence of, for example, height of vertical load, lateral load eccentricity, warping fixity, and geometric imperfections (of various types). There is, of course, a necessity to understand the effect on buckling resistances and member deformations of the combination of all the above-mentioned influential variables, together with imperfections from the variable distribution of material properties.

The contribution to knowledge presented herein endeavors to explore and understand the responses of a single PFRP I-section (120x60x6 mm) from Fiberline Composites A/S (now

Fiberline Building Profiles), in Denmark, subjected to three-point flexure that fails with the elastic instability mode of Lateral-Torsional Buckling (LTB) in the presence of combined influences from changes to: vertical load height; lateral loading eccentricity; geometrical imperfections; end displacement boundary conditions. Further background and detailed information on this research are presented in the PhD thesis by the first author [6]. The imperfection owing to the variable distribution of E_L is a constant modelling parameter. ABAQUS® is the commercial simulation software employed for the Finite Element (FE) sensitivity analyses, which are conducted by modelling changes that involve five beam spans, two different end conditions to the simply supported beams, three vertical load heights, nine lateral load eccentricities and three types of geometrical imperfection. Initial FEs analyses using ABAQUS® are with Eigenvalue solutions for the elastic critical buckling loads. To rigorously analyze the LTB responses of the PFRP beams with combinations of variables, most FE analyses are of the geometrical nonlinear type. Because PFRP material is linear elastic for strains to LTB failure, the modelling methodology does not involve material nonlinearity.

2. Numerical Modelling Methodology and Problem Definition

The degree of numerical accuracy (in terms of the computational results) is affected by the choice of modelling using ABAQUS® capabilities that includes element type; meshing density, the criteria for material failure (based on material strength components and stress interactions) [2, 3, 5 and 19]. There are various material failure criteria for laminated composites, with popular Tsai-Hill [20 and 21] and Hashin Damage Initiation [22-24]. Such failure predictors are used, see [25-28], to investigate the structural responses of PFRP sections when ultimate failure is governed by material failures. In the present study we use linear elastic analyses to evaluate elastic buckling loads and corresponding deformed shapes linked to the LTB mode of failure of flexural members. To investigate PFRP beams failing in LTB our FE work does not need to introduce any nonlinear material behaviours (e.g., for initiation and progressive crack

growth); it only needs to consider geometrical nonlinear deformations associated with LTB instabilities.

2.1 Choice of Numerical Modelling

In general, ABAQUS® [29] offers three options to model the laminated panels in thin-walled PFRP sections, and they can be classified as the:

(i) 'microscopic' option, where matrix and fibre reinforcement constituents are modelled separately. This option is complex because it requires the analyst to know of the actual distribution of fibre reinforcements and mechanical properties such as: strength and toughness of the fibre-matrix interface; individual fibres; matrix materials; cohesive energies. It can only be used in FE modelling and simulations of relatively small volumes, and then the cost of computation can be very high. In terms of problem solving this option can be employed to analyse crack propagation and debonding between fibres.

(ii) 'macroscopic' option where the laminated panels are modelled as a single layer of orthotropic material with directional mechanical properties. This option is suitable for the modelling and simulation of the overall structural behaviour of structural members. In terms of input data it requires knowledge of the following material properties or elastic constants (obtained by standard test methods): the Longitudinal modulus of elasticity, E_L; the Transverse modulus of elasticity, E_T; the in-plane shear modulus, G_{LT}; the Major Poisson's ratio, v_{LT}.

(iii) 'combined' option, in which the thin-walled laminated panels are modelled by a number of discrete 'macroscopic' orthotropic layers, each of constant thickness within the panel. This option also, like option (i), requires individual properties for fibre architecture per layer, and for the matrix and fibre reinforcement constituents.

Of the above-mentioned three options that of (ii) for the 'macroscopic' approach is deemed appropriate and sufficient to obtain numerical predictions to understand the overall structural behaviour of PFRP members subjected to flexural deformation. By way of his PhD work, Nguyen [6] found this option for modelling PFRP material properties to be the most numerically reliable in terms of FE modelling and computational efficiencies.

2.2. Geometric and Material properties

Previous numerical studies, such as [30] and [31] have found that LTB failure of PFRP beams will occur when the maximum longitudinal strains are within the linear elastic range. Experimental studies [2] and [6] also confirm this physical fact for the modelling methodology to involve linear elastic material.
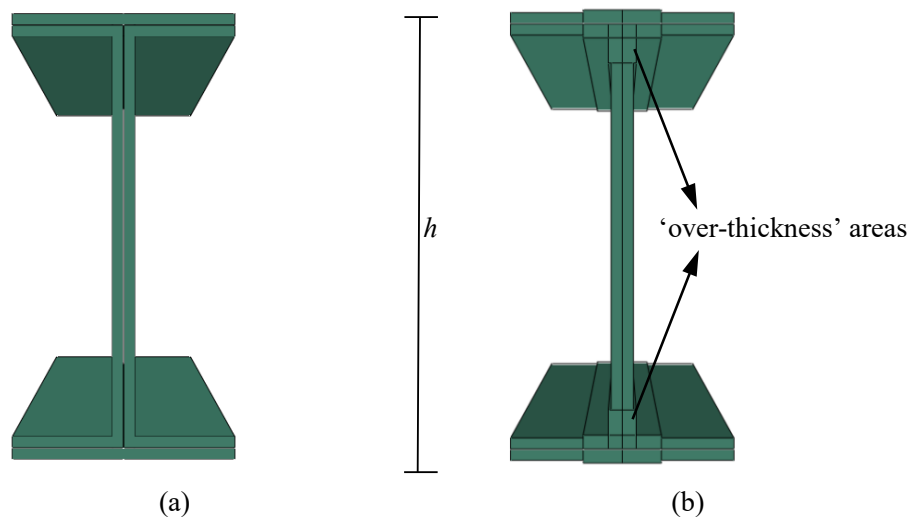

Figure 1. Modelling of the geometry an I-section: (a) ignoring presence of fillet radii volumes; (b) accounting for material in the fillet radii volumes.

The element type and meshing density were chosen by Nguyen [6] based upon evaluations of FE bifurcation buckling loads that can be compared with analytical predictions using closed-form formula solutions. The numerical predictions for LTB resistances were obtained from conducting eigenvalue analyses. It is noted that in this FE study the fillet volumes (for the junctions between flange and web) in I-sections were included in the meshing of the beam's

volume for sectional properties. Shown schematically in Figs. 1(a) and 1(b) is the change from modelling of a I-section of depth h, without and with, respectively, the presence of the fillet volumes, which will, for example, increase the second moment of area about the axis of flexure and the torsional constant associated with failure in the LTB mode.

In general, PFRP laminated panels [1] can be modelled for their elastic constants as either orthotropic or transversely isotropic [32 and 33]. An orthotropic material has three mutually orthogonal axes for different directional material properties. Transversely isotropic material is a special case of an orthotropic material, in which the transverse plane is a plane with isotropic properties. By denoting '1' for the (longitudinal) direction of the laminate (with the highest proportion of unidirectional fibres), '2' for the transverse direction (in the plane of the laminate and perpendicular to '1' direction), and '3' for the through-thickness direction, the definition of an orthotropic material involves nine independent elastic constants namely: three moduli of elasticity (E_1, E_2, E_3), three shear moduli (G_{12}, G_{13}, G_{23}), and three Poisson's ratios (ν_{12}, ν_{13}, ν_{23}). If the distribution of fibres in the 2 and 3 directions is the same, the material is transversely isotropic and the elastic constants reduce to five [33].

PFRP sections comprise of laminates having alternative reinforcing layers of continuous unidirectional fibres and fibre mats (in which continuous fibres can be randomly and uniformly distributed). It is acceptable to assume that these laminates are transversely isotropic [2, 18, and 31], and for FE modelling the five independent elastic constants are E_1, E_2, ν_{12}, ν_{23} and G_{12}. By noting the '1'-direction as the Longitudinal direction in pultrusion and the '2' direction as the Transverse direction there is the association that E_1, E_2, G_{12}, ν_{12} can be written as E_L, E_T, G_{LT}, ν_{LT}.

The simplest modelling option to define a transversely isotropic material with ABAQUS® is to specify the 'nine' engineering constants of: E_1, $E_2 = E_3$, ν_{12}, $= \nu_{13}$, ν_{23}, $G_{12} = G_{13}$, G_{23} with E_2

$= 2G_{23}(1 + v_{23})$. Under plane stress conditions, as is the formulation of shell finite elements in ABAQUS®, only the elastic constants in the L-T plane (i.e., E_L, E_T, G_{LT} and v_{LT}) are required for input modelling data [33]. Shear moduli G_{TL} and G_{TT} are only important in modelling should the computational analysis require the determination of transverse shear deformations [34]. For PFRP materials, the Poisson's ratio v_{TT} is a matrix dominant elastic constant that is known to be > 0.35 [33]. By letting this Poisson's ratio equal 0.35 the shear modulus G_{TT} can be specified by $E_2/2.7$.

Taken from [6] are the measured mean elastic constants summarized in Table 1 for an I-section of glass fibre reinforcement and a fire retardant vinylester based matrix. The nominal size of this section, a standard profile pultruded by Fiberline Composites A/S, is 102x60x6 mm. For the six panels (four flange outstands, labelled I1 to I4) and two web sub-panels, labelled I5 and I6) in the I-section columns (1) to (6) in Table 1 report their elastic constants for a constant parameter input data in the ABAQUS® FE models.

Table 1. Elastic constants for flange and web panels in Fiberline Building Profiles Composites' I-sections 120x60x6mm
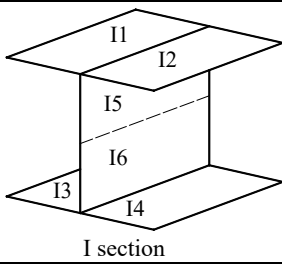
Shape	Flange I1	Flange I2	Flange I3	Flange I4	Web I5	Web I6
I section						
$E_L = E_1$ (GPa)	34.4	29.7	34.5	31.2	26.3	26.2
$E_T = E_2$ (GPa)	N/A	N/A	N/A	N/A	10.8	10.8
$G_{LT} = G_{12}$ (GPa)	N/A	N/A	N/A	N/A	4.2	4.2
$G_{TT} = G_{23}$ (GPa)	N/A	N/A	N/A	N/A	4.0	4.0
$v_{LT} = v_{12}$	0.23	0.25	0.24	0.21	0.22	0.23

Table 1 reports that the I-section possesses different tensile values of Longitudinal modulus of elasticity, E_L, in the four flange outstands (at 29.7 to 34.5 GPa) and two web sub-panels (at 26.2 and 26.3 GPa). The Transverse modulus of elasticity, E_T, at 10.8 GPa was only measured using web material, and this limitation is not important because the influence of changing E_T to carry out the sensitivity studies on LTB resistance is insignificant. It is shown in [6] that a change of 30% in E_T will reduce or increase LTB resistance by only < 1%. This finding is because the transverse modulus does not contribute to the governing stiffnesses of flexure and torsional for the LTB response. Major Poisson's ratio ν_{LT} is found to lie in the narrow range 0.21 to 0.24. In-plane shear modulus G_{LT} at 4.0 GPa was measured using web material only [6]. It is acceptable in this FE work to assume that the flange outstands have the same E_T and G_{LT} as measured for the web.

The choice of finite element type is between solid and shell. Shell elements are popular for thin-walled structural problems, in which through-thickness effects, such as shear stresses, can be neglected. Compared with using solid elements, a modelling methodology with shell elements is generally simpler and the mesh specification based on elements located on the mid-depth planes of the panels is more straightforward to specify, generate and change in a sensitivity study. In terms of computational resourcing, shell elements are timesaving because they enable modelling with many fewer elements (and many fewer degrees of freedom) than when meshing the same volumes with solid elements. Application of solid elements is necessary when the objective of the FE analysis is, for example, to determine structural failure, say owing to: through-thickness fracture; in-plane delamination damage; the presence of joints and connections. Because no material failure is to be modelled and simulated in this FE work it is appropriate to use shell elements, and it is observed that a similar shell element modelling approach for instability analyses of PFRP members have been used by other researchers [25-28].

With ABAQUS® the three shell element types of S4R, S4R5, and S8R are commonly adopted for Eigenvalue buckling analyses [35-38]. For general-purpose modelling, the four-noded linear elastic shell elements S4R and S4R5 apply linear shape functions to interpolate deformations between nodes and are suitable for representing both thin and thick shell elements [34]. The '5' in element type S4R5 is because each node has 5 degrees of freedom by ignoring the degree of freedom for rotation about the axis normal to the shell's element mid-surface. This specific element formulation improves computational efficiency. Thick shell element S8R employs quadratic shape functions by having eight nodes per element and the formulation for the element stiffness matrix adopts the Mindlin plate theory for first-order shear deformation. Between adjoining element sides element S8R has displacement compatibility that avoids there being any displacement discontinuities. These finite element attributes are known to give higher numerical accuracy when the mesh specification is coarser [39]. The 'R' in element types S4R and S8R denotes that the number of Gaussian integration points is Reduced. This is another finite element formulation attribute known to improve computational efficiency, as well as avoiding the modelling and numerical problem of shear locking [34].

The pultruded I-shape in the numerical study has cross-section of 120×60×6 mm. The beam's span is 1500 mm with the simply supported end conditions imposing torsion to be fully restrained. As introduced earlier, the elastic constants for LTB load predictions are those listed in Table 1. Eigenvalue analyses were carried out with this beam example subjected to a point vertical load at mid-span, and at the shear centre. The objective of this study is to be able to compare the numerical performances of the three shell elements S4R, S4R5 and S8R against resistance predictions using the closed-form formulae for LTB given in [40], noting that the end boundary conditions are for $k = k_w = 1.0$; k and k_w are the effective length factors for lateral flexure and warping, respectively. The closed-form solution by Kollár and Springer [40] is for LTB of beams of orthotropic (and thereby transversely isotropic) materials. It was formulated

by exchanging the force-strain relationships for isotropic materials with those for orthotropic material. It is relevant to this study because it also accounts for the reduction in LTB resistance due to the influence of shear deformation, which the ABAQUS® elements will inherently provide. It is noted that the reduction will be highest for wide-flange beams (when flange breadth dimension equals the section's depth dimension) and/or for laminates having a relatively high ratio of E_L/G_{LT} (which can be up to 80 when fibres are of carbon). For this study with a narrow-flange I-beam of PFRP (E_L/G_{LT} is 8 to 10), the maximum load reduction at LTB instability is about 5%.

Equation (1) is for the closed-form solution, without shear deformation, for the elastic critical buckling load (kN), P_{cr}, for simply support pultruded beams (with $k_w = 1.0$):

$$P_{cr} = \frac{4M_{cr}}{L} = \frac{5.39\pi^2 E_L I_z}{L^3}\left(\sqrt{\frac{I_w}{I_z} + \frac{L^2 G_{LT} I_T}{\pi^2 E_L I_z} + 0.40z_g{}^2} - 0.63z_g\right) \tag{1}$$

In Eq. (1) the geometrical properties for the I-beam are: L is for the span (mm); I_z is for the second moment of aera for flexure about the minor-axis (mm^4); I_w is for the warping rigidity (mm^6); I_T is for the torsional rigidity (mm^4). Parameter z_g is for the height of the load from the shear centre. z_g is zero at the shear centre and positive when above (towards top flange) and negative (towards bottom flange) when below.

Because it is known that the difference in elastic critical buckling loads with the shear deformation solution or from Equation (1) is not significant, see [41], the effect of shear deformation on LTB resistance can be ignored in this numerical study.

2.3 Mesh Sensitivity Analysis, Web-flange junction modelling

On taking the mean values from the testing (see Table 1) for the elastic constants we have E_L = 30.4 GPa and G_{LT} = 4.2 GPa in the closed-form equation in [40], with shear deformation, to

predict $P_{\text{cr,sh}} = 7.6$ kN. The same beam parameters are modelled in an ABAQUS® Eigenvalue

analysis for LTB resistance, noting that the inputted elastic constants taken from Table 1 are:

E_L (or E_1) = 30.4 GPa; E_T (or E_2) = 10.8 GPa; G_{LT} = G_{12} or G_{13} = 4.2 GPa; $\nu_{LT} = \nu_{12} = 0.2$; G_{TT}

= G_{23} = 4.0 GPa. A mesh sensitivity analysis is conducted by the authors for each of the three

element types to check convergence of the numerical predictions. Table 2 reports in columns

(3) to (5) the elastic critical buckling loads, $P_{\text{cr,FEA}}$, for the element types with varying mesh

size. The number of elements per m of span are given in column (2) with in column (1) are the

element lengths in millimetres in the spanning direction. The size and number of elements in

the models are varied by changing the side aspect ratio when meshing the 30 mm wide flange

outstands and 114 mm deep web. For the flange outstands the element dimensions are: 5×5

mm; 10×10 mm; 15×15 mm; 30×30 mm, or 6, 3, 2 or 1 elements across an outstand width

dimension. Whilst for the web the element sizes are: 5.18×5 mm, 9.5×10 mm; 14.25×15 mm;

28.5×30 mm, or 22, 12, 8 or 4 elements in the depth dimension.

Table 2. Elastic LTB loads for three shell element types with mesh refinement

Element side length in span direction (mm)	Total number of elements per m span	$P_{\text{cr,FEA}}$ (kN) S4R5	$P_{\text{cr,FEA}}$ (kN) S4R	$P_{\text{cr,FEA}}$ (kN) S8R
30	2567	6.15	6.15	7.48
15	1067	7.16	7.15	7.45
10	2400	7.34	7.32	7.45
5	9200	7.42	7.41	7.44

From inspection of the changing $P_{\text{cr,FEA}}$ in the table it can be observed that there is an

insignificant (< 3%) change when the element side length with elements types S4R5 and S4R

is < 15 mm, and convergence with mesh refinement is to $P_{\text{cr,FEA}} = 7.4$ kN (to nearest 0.1 kN).

This is 4% lower than, $P_{\text{cr,sh}}$, with shear deformation, by way of the closed form formula [40].

Showing a loss in numerical reliability is the reduction in $P_{\text{cr,FEA}}$ by 16% on doubling the side

length to 30 mm. The best performing element type is S8R, which gives the most reliable set of $P_{cr,FEAS}$ with range from 7.48 to 7.44 kN and differences of < 1%. Because of its superior numerical performance, this ABAQUS® double-curved thick shell element with meshing side length of maximum 15 mm, is adopted in all following numerical sensitivity studies.

Geometry modelling of an I-section without a corner fillet radius is illustrated in Figure 1(a). This modelling geometry is acceptable when the fillet radius at the flange/web junctions is relatively small and/or when the torsional constant, I_T, is not an influential parameter in how the loaded member response to loading. For the LTB failure mode, the magnitude of I_T plays a significant role because it controls the torsional stiffness term in the lateral-torsional deformation; refer to the second term of $G_{LT}I_T$ under the square root in Equation (1). Calculations for I_T in [6] shows that for the Fiberline Composite profile 120x60x6 mm the four fillet radius volumes cannot be ignored. By introducing their areas into the section properties it is found by Equation (1) that P_{cr} increases by 15% higher [42 and 43]. This result translates to the four fillet radius volumes being introduced into the FE work for the sensitivity studies for elastic critical buckling loads. An appropriate modelling approach to compensate for the 'losses of fillet radii material is presented in [44] and [45]. Practically, the four 'volumes' along the I-section's length in the mesh are assigned to shell elements having increased (constant) thicknesses, as illustrated in Figs. 1(b) and for the profile 120x60x6 mm with the meshing dimensions in Fig. 2.

Figure 2 shows the modification to the flange outstand and web 'constant' thicknesses of 6 mm to develop the junction volumes. As illustrated, the original thickness of 6 mm is increased by 1.5 mm to 7.5 mm over a width of 21 mm in a flange and over a height of 10.5 mm (from the mid-plane of the flange) at both ends of the web. This updated geometrical modelling increases I_T by 28% (to 2.15×10^4 mm^4) [6], with accompanying smaller increases of 3% and 0.4% in the

warping constant, I_w, and the second moment of area about the minor-axis, I_z. The latter increases in geometrical properties I_w and I_z do not have a significant effect on P_{cr}; the 15% increase from using Equation (1) is solely due to the dramatic change in the torsional constant.
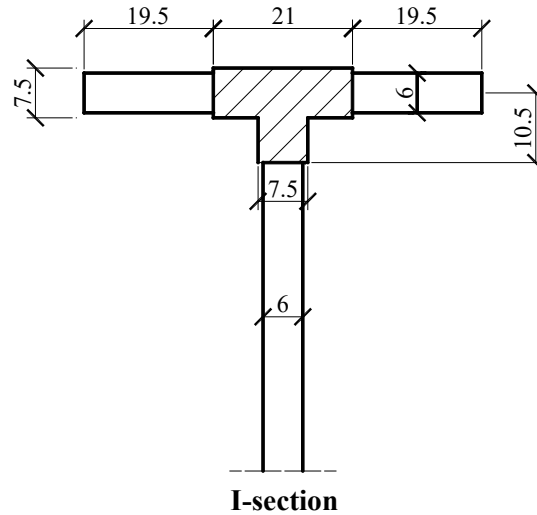

I-section

Figure 2. Changes in thicknesses in the region of the web-flange junction to account for fillet radius volumes.

For a sensitivity study on LTB resistance with changing vertical height of the central point load requires P to be applied: on the top surface of the Top Flange (TF); at the Shear Centre (SC); on the bottom surface of the Bottom Flange (BF). By default, the shell element modelling uses the mid-thickness plane for the vertical web as the reference plane for loading. Because of this modelling feature the top or bottom flange load cases would inherently place, P, at half-flange thickness (which is 3 mm) below the flange's outermost surface. ABAQUS® [29] has the modelling option to define a distance from a reference surface where the nodes to apply forces and moments are located. This enabled a modelling modification to be made by constructing a reference surface for both top and bottom flanges so that P is applied with $z_g = +h/2$ (top flange) and $z_g = -h/2$ (bottom flange) from the shear centre of the I-section (where $z_g = 0$).

2.4 Different End Conditions

ABAQUS® FE analyses are carried out with two different displacement boundary conditions at the end supports, which are named End Conditions 1 (EC1) and End Conditions 2 (EC2). EC1 conditions allow for 'free' warping and 'free' minor-axis rotation at both ends. This simulates the end conditions having a lower LTB resistance compared to any other simply supported (for major-axis flexure) end conditions and is thereby the most conservative calculated resistance. Conditions EC2 allow for 'free' warping but is 'fixed' for minor-axis rotation owing to minor-axis flexure. EC1 and EC2 conditions are those that were implemented in a physical testing programme by Nguyen [6], with the EC2 achieved by effectively clamping ends to lateral flexure of the beam. Figure 3 shows an end of the beam with a Cartesian coordinate system for the FE modelling. The labelling defines the three translational (U_x, U_y, U_z) and three rotational displacements (UR_x, UR_y, UR_z) that are be specified to model displacement boundary conditions EC1 and EC2. The schematic drawings in Figs. 4 and 5 introduced the end conditions in the physical testing that satisfy EC1 and EC2, respectively.
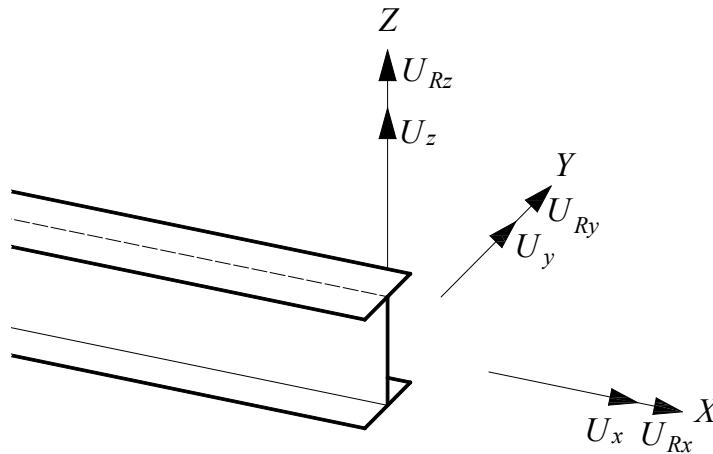

Figure 3. Cartesian coordinate system in FE modelling.

Fig. 4 shows that EC1 is realized by having one pair of vertical steel rods in contact with both sides of the I-section at the ends, and the photograph in Figure 6(a) shows this test set-up. In the FE modelling the EC1 boundary conditions are simulated, as shown in Figure 6(b), by restraining the horizontal movement ($U_y = 0$) at four nodes in a section plane, with one node in

each flange outstand. These nodes represent the contacting points between the I-section and the steel supporting rods. The roller end for the simply support condition is modelled by imposing the restraint for vertical movement, $U_z = 0$, over the contacting area. At the other end where the beam is fully restrained from translation along its axis, both U_z and U_x are set equal to zero.
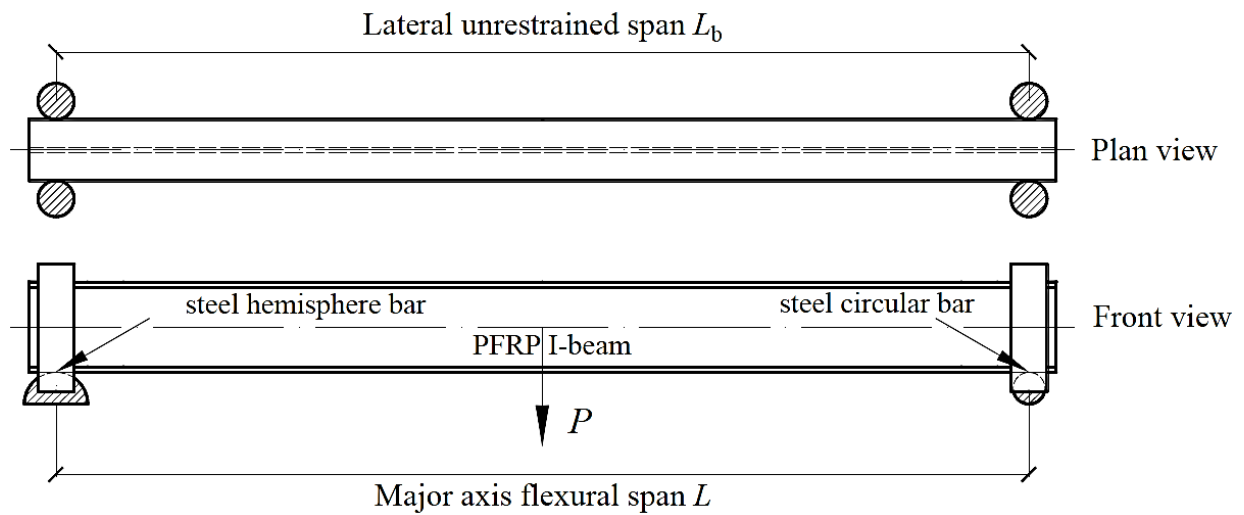
Figure 4. Schematic drawing for test set-up with end boundary conditions EC1; note that lateral unrestrained span L_b equals the major-axis flexural span L.
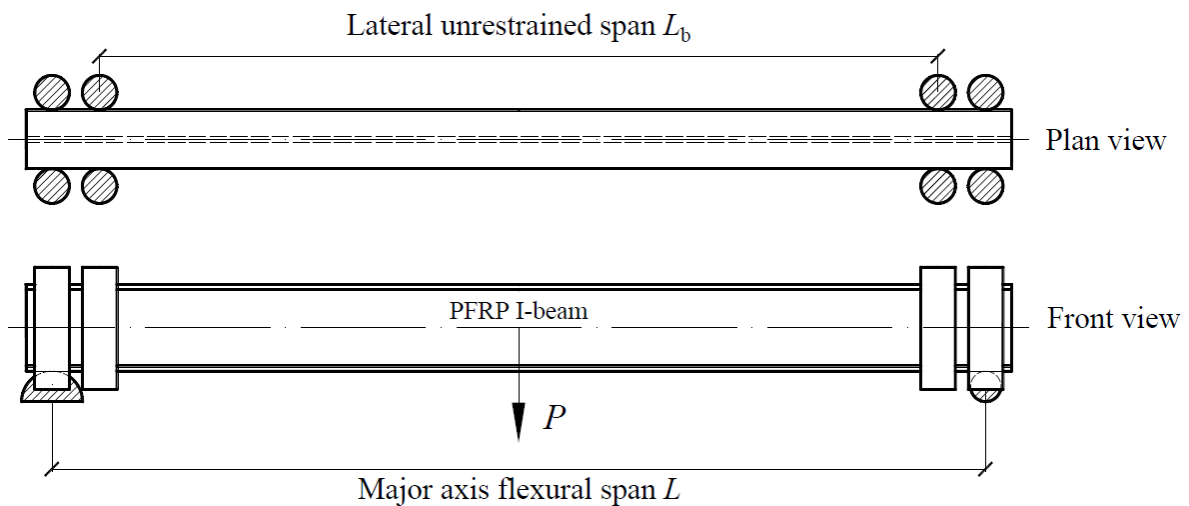
Figure 5. Schematic drawing for test set-up with end boundary conditions EC2; note that lateral unrestrained span L_b is < major-axis flexural span L.
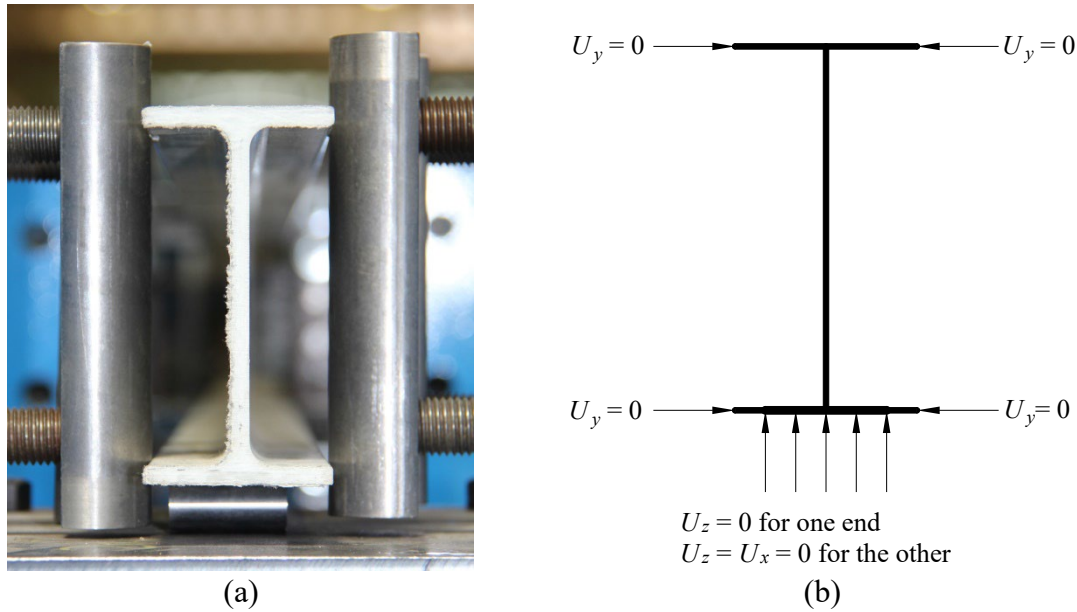
Figure 6. Arrangement of EC1 for I-section in: (a) testing; (b) FE modelling.

To model the EC2 condition the EC1 displacement restraints have the addition of restraining at the position of the second vertical roller the horizontal movement ($U_y = 0$) at four nodes in a section plane, with one node in each flange outstand.

2.5 Lateral Torsional Buckling loads

To characterize LTB loads both linear Eigenvalue and geometrical nonlinear analyses are employed. Eigenvalue analyses predict the elastic critical buckling loads, $P_{cr,FEAS}$, for bifurcation failure based on the unloaded beam geometry. By applying geometry perturbations in the meshed geometry, and looking for local and/or global deformations that, owing to second-order effects, might promote the onset of LTB instability, this FE simulation approach gives load factors (the Eigenvalues) for buckling loads. To obtain $P_{cr,FEA}$ the input load in the model is multiplied by the ABAQUS® load factor. The associated eigenvector to each Eigenvalue establishes the corresponding deformation mode shape, which is defined by a normalized vector for nodal displacements on setting the maximum nodal displacement

component to 1.0 [46]. For an Eigenvalue analysis the mode shape only shows how the beam buckles, it gives no results on the load-deflection response.

To extract Eigenvalues ABAQUS® provides the two solution methods of Lanczos and Subspace iteration, with the latter being the default solver [29]. Subspace iteration is effective computationally for calculating a small number of eigenmodes, whilst the Lanczos method is expected to be more resource efficient when a larger number of eigenmodes are required for structural systems possessing many degrees of freedom [46]. Because this study need only focus on the first few modes for LTB failure the subspace iteration approach is employed.

For geometrical nonlinear analysis the actual load-deflection response predicted by applying P in small increments and calculating the current (static equilibrium) deformation state at each load increment. The FE deformations follow the beam loading until instability occurs (imperfection initiated), and this corresponds closer to practice and what is observed in a physical testing programme, such as detailed in [6]. Because the pultruded material is linear elastic [1] there is no material nonlinearity. It is noted that this modelling assumption remains appropriate, providing loading (to failure) is short-term and deformations from viscoelasticity remains negligible, which is acceptable for the test programme presented in [6].

ABAQUS® solves a geometrical nonlinear problem by employing a modified Riks method [47]. To cope with structural nonlinearity this is a commonly used numerical method, known also as the arc-length method, originally derived by Riks and was improved for computational efficiency by Crisfield [48]. Since post-buckling responses are not being studied the nonlinear analyses are terminated after a few load increments when the beam become unstable and overall deformations are found to be progressing into the post-buckling region.

To investigate the influence of the governing imperfection on the LTB response of the PFRP I-beams an initial minor-axis out-of-straightness is introduced into the FE model for spans, L,

from 1900 to 4100 mm, by assuming the centreline of the I-beam follows a sinusoidal wave with maximum imperfection, δ_{max}, at mid-span. This imperfection linked to lateral flexure is expressed by $\delta_{max} \sin(\pi x/L)$, where x is a distance along the length of the beam. It is introduced into the beam's mesh, as shown by the (exaggerated) deformed shape from an Eigenvalue analysis in Figure 7, by modifying the nodal coordinates through the adoption of a vector field [6]. It is note that the modified shapes for the five spans reported in Table 3 were obtained by scaling the first Eigenvalue buckling mode shape for Euler buckling of a perfectly straight concentrically loaded column.
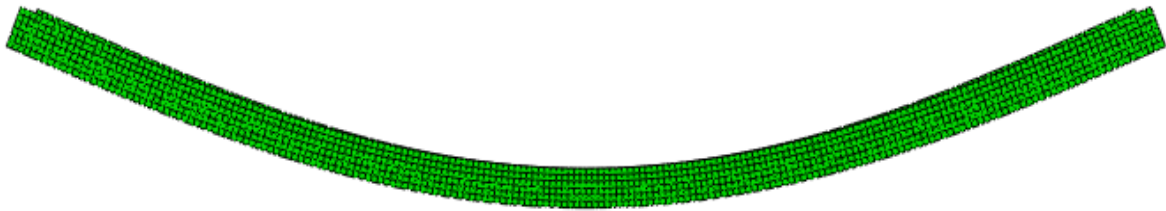

Figure 7. Minor-axis out-of-straightness imperfect shape in FEA (exaggerated).

Table 3. Minor-axis maximum out-of-straightness with span L

Span, L (mm)	I-section	
	δ_{max} (mm)	L/δ_{max}
1900	0.78	2435
2500	2.86	874
3000	1.95	1538
3500	2.72	1286
4100	2.66	1541
Average	2.19	1535

The values of δ_{max} used for this geometric imperfection at five spans were measured by Nyugen [6]. They are summarized in Table 3, with the average maximum being $L/1535$. Relative to the original straight beam the minor-axis initial curvature can be for two imperfection modelling options (or directions), as illustrated in Fig. 8.
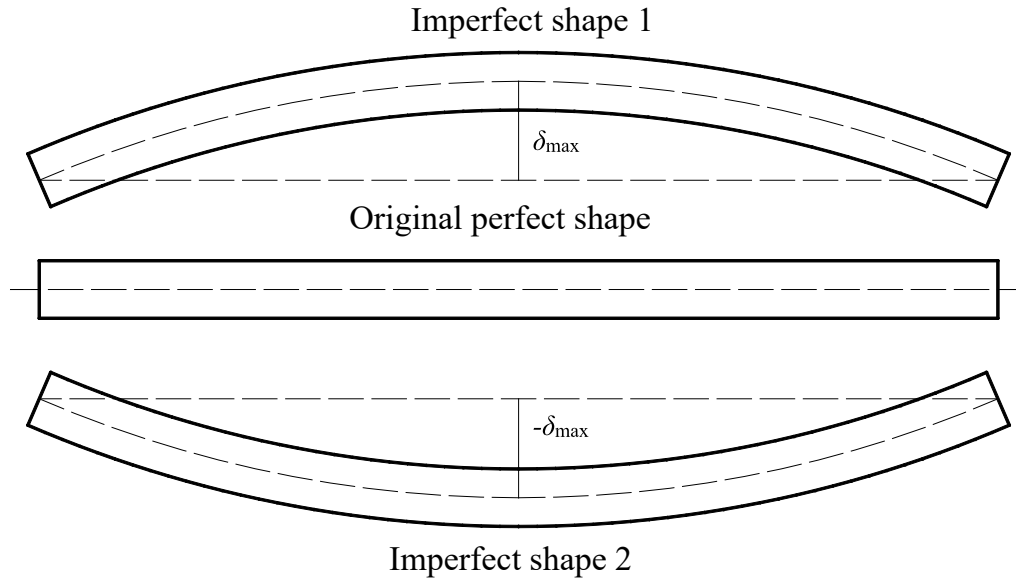
Imperfect shape 1

Original perfect shape

Imperfect shape 2

Figure 8. Two imperfection options of the minor-axis out-of-straightness for lateral flexure.

3. Results for Influence of material and geometric imperfections

Nonlinear analyses were carried out with the imperfection shapes shown in Fig. 8 and the other variable parameters being the three vertical loading cases of: top flange (TF); shear centre (SC); bottom flange (BF). As an example, of the adopted labelling, the model EC1_3500_SC is for the beam having End Conditions 1, a span L of 3500 mm (Table 3), and the vertical point load applied at Shear Centre of the I-section (and always at the mid-span). For a geometrical nonlinear analysis Figure 9 presents a typical plot of predicted load P with vertical deflection, w. Owing to the influence on beam deformation of the minor-axis out-of-straightness the curve goes nonlinear and there is no bifurcation point, which in an Eigenvalue buckling analysis defines the elastic critical buckling load, $P_{cr,FEA}$. It can be shown that, for any specific beam configuration, the bigger the initial imperfection is, the lower will be P at the same w, and it's not straightforward to quantify the imperfection sensitivity on LTB resistance. The influence of having the governing imperfection associated with lateral flexure is that under increasing, P, there is a progressive loss in flexural stiffness as the beam twists and bend laterally. Figure 9

shows that the buckling load from nonlinear analyses cannot be $P_{\text{cr,FEA}}$, and that it is to be defined by the limiting value $P_{\text{Limit,FEA}}$.
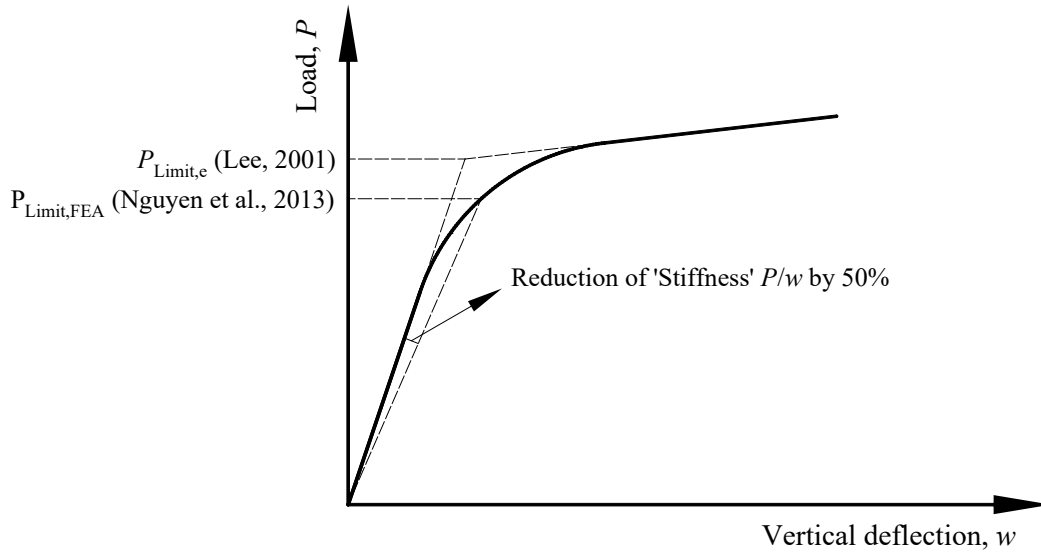

Figure 9. Definitions of limiting buckling load in Lee [42] and Nguyen *et al*. [4] and [43].

Nguyen in [6] and [50] proposes a 'stiffness reduction method' to establish what is $P_{\text{Limit,FEA}}$ and this method is illustrated in Figure 9, together with the 'tangent method' of Lee [49]. The new definition for $P_{\text{Limit,FEA}}$ comes from the observation that, in nonlinear analyses, the flexural stiffness P/w is observed to only vary slightly during pre-buckling. $P_{\text{Limit,FEA}}$ is taken as the value of P at which the secant stiffness is reduced by 50% (and we call this the 'transition point' between stable and unstable static equilibrium).

Clearly, to apply the method in data reduction following physical testing requires precise readings for vertical deflection, w. Satisfying this requirement in practice is technically challenging because when there is LTB failure the readings from two displacement transducers, at mid-span (and originally measuring vertical movement via the top and bottom flange) cannot give the exact vertical displacement at the shear centre. To therefore obtain reliable values of $P_{\text{Limit,FEA}}$s from test results, the method adopted by Nguyen [6] is equivalent to that applied by

Stoddard [1], who used measured load-rotations (P/ϕ) and a limiting angular of rotation (twist) for a specified reduction in torsional stiffness.
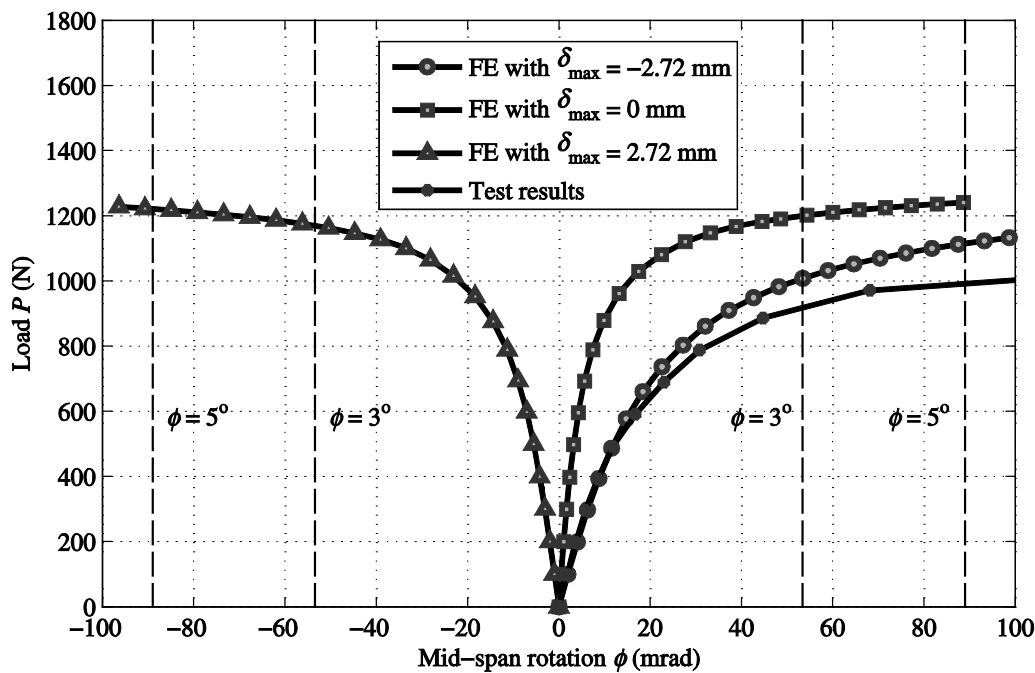

Figure 10. P vs. ϕ curves for beam EC1_3500_SC.

Figure 10 shows four plots of load P with mid-span rotation ϕ for beam EC1_3500_SC. The plots with circular, square, and rectangular symbols are from FEA having the three different imperfection types (refer to Table 3 and Figure 8), and they are compared with the physical test results taken from [6]. It is observed from testing (the curve on the right side with lowest P) that at $\phi = 5°$ (or 82.7 mrad), the beam has deformed significantly into the LTB post-buckling region. At this angle of twist of the mid-span cross-section the FE generated curves are observed to have reached ultimate load and the beam's rotational stiffness is negligible. Based on engineering judgment, the $P_{Limit,FEA}$'s reported in Tables 4 and 5 have been established from the P with ϕ curves at the constant $\phi = 3°$. Note that for the limiting load determined from a physical test [6], again when $\phi = 3°$ the notation in the tables is $P_{Limit,e}$.

Table 4. Limiting buckling loads for FEA (with different δ_{max}) and tests for EC1

Span (mm)	Top Flange (TF) $P_{Limit,FEA}$ (kN)			$P_{Limit,e}$ (kN)	Shear Centre (SC) $P_{Limit,FEA}$ (kN)			$P_{Limit,e}$ (kN)	Bottom Flange (BF) $P_{Limit,FEA}$ (kN)			$P_{Limit,e}$ (kN)
	$-\delta_{max}$	0	$+\delta_{max}$		$-\delta_{max}$	0	$+\delta_{max}$		$-\delta_{max}$	0	$+\delta_{max}$	
1828	3.38	3.61	3.86	3.48	4.62	4.97	5.36	5.96	6.91	7.50	8.10	8.64
2438	1.56	1.93	1.81	2.10	2.05	2.58	2.44	2.50	2.80	3.52	3.39	3.83
2844	1.27	1.45	1.48	1.55	1.66	1.92	1.97	2.00	2.25	2.62	2.74	2.60
3454	0.81	0.95	0.92	0.96	1.00	1.20	1.17	1.04	1.28	1.53	1.51	1.33
4064	0.62	0.72	0.70	0.57	0.76	0.90	0.88	0.72	0.96	1.15	1.13	0.83

It can be seen from the three FE-generated P with ϕ curves in Figure 10 that when $\delta_{max} = 0$ (curve with open square symbol) the beam has the same progressive twist to instability as predicted when $\delta_{max} = \pm 2.72$ mm. Furthermore, with the same imperfection magnitude of 2.72 mm but in the opposite directions the P vs. ϕ curve (open triangle symbol) is not identical (in absolute terms). The engineering reason for this is because the I-section has different elastic constants in the four flange (and two web) panels. Had there not been an imperfection seeded into the FE model to simulate the variable distribution in E_L there would be no $P_{Limit,FEA}$ prediction when $\delta_{max} = 0$. An important finding from the plots in Figure 10 is that that the curve (open circle symbol) from the FE model with $\delta_{max} = -2.72$ mm is comparable with the experimental generated curve (filled circle symbol).

Figure 11 presents the same plotting of P ϕ curves as in Figure 10 for beam EC1_1900_TF. The test results are plotted as the discontinuous curve with filled circle symbol. It is observed for this shorter span beam with Top Flange loading that when $\delta_{max} = +0.78$ mm (triangular symbol) the highest $P_{Limit,FEA}$ is realized. This observation is similar what we have from the FE

results plotted in Fig. 10 for EC1_3500_SC and is for the recognition that combinations of imperfections (here geometrical and material) can create a loaded beam set-up producing a better response than had the beam, say, no out-of-straightness imperfection. It is seen from the FE curves in Figure 11 that the lateral movement for LTB deformation is in the same direction when δ_{max} = +0.78 mm, δ_{max} = 0 mm (curve with open square symbol) or δ_{max} = -0.78 mm (curve with open circle symbol). Because this response is not found with the curves for beam EC1_3500_SC in Figure 10 it can be attributed to the difference in span and relative magnitudes of the combined imperfections.
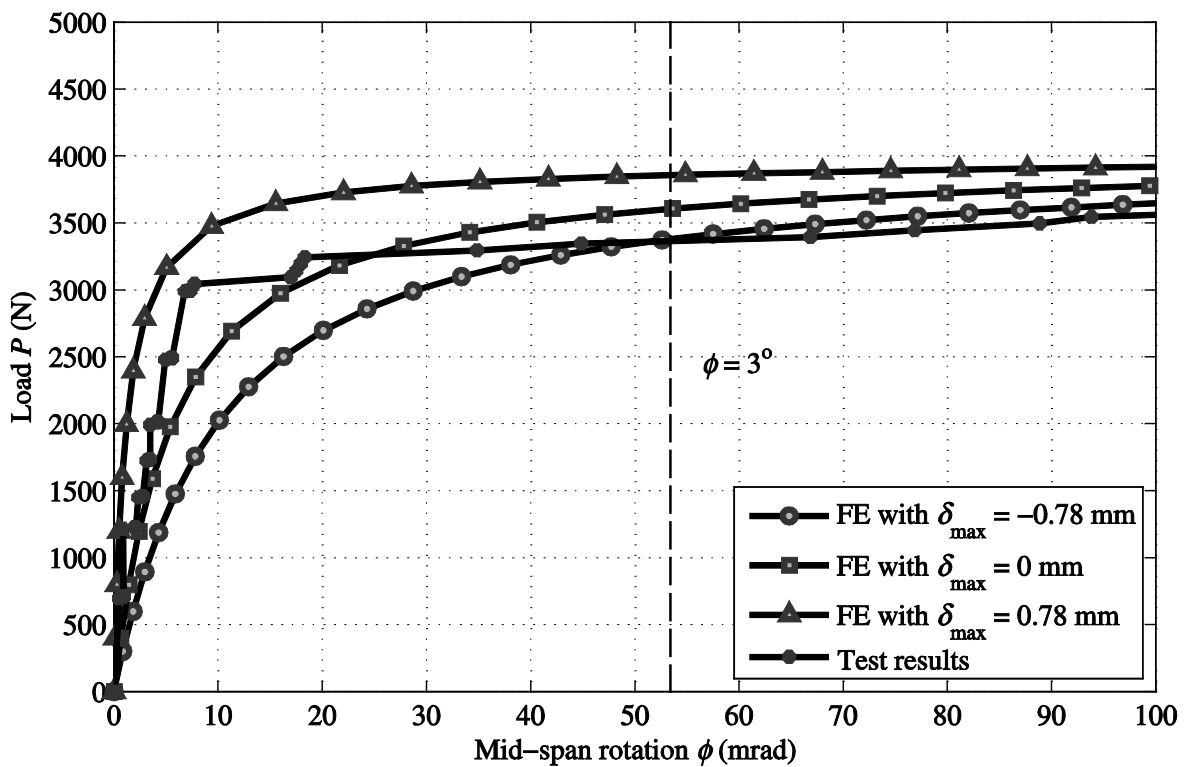

Figure 11. P vs. ϕ curves for beam EC1_1900_TF.

Presented in Tables 4 and 5 are values of $P_{Limit,FEA}$ with their $P_{Limit,e}$s for the five beam spans (Table 3) and either EC1 or EC2 end conditions, respectively. The tabulated predictions provide a direct comparison for the single pultruded I-beam having: five different spans, three

different loading cases of Top Flange (TF), Shear Center (SC) or Bottom Flange (BF); three different geometrical imperfections, namely $-\delta_{max}$, 0 and $+\delta_{max}$. Both tables have the following format. Column (1) lists the beam spans in the range 1828 to 4046 mm; the depth of the I-section is 120 mm. Next, we observe that columns (2) to (4), columns (6) to (8) and columns (10) to (12) are reporting $P_{Limit,FEA}$s for the three δ_{max}s. The change between these three groups of 15 $P_{Limit,FEA}$ results is that they are for, respectively, top flange, shear centre and bottom flange load cases. For the same left-to-right entry order for vertical load height, columns (5), (9) and (13) report the experimental limit loads, $P_{Limit,e}$s.

By comparing the $P_{Limit,FEA}$s at each loading case, it is observed that, as expected, the value of δ_{max} has a significant influence on the predicted LTB resistance. The difference between the highest and lowest resistance (in terms of lowest of three predictions) is for: TF_EC1 between 7 and 24%; SC_EC1 between 8 and 26%; BF_EC1 between 8 and 22%. As expected, $P_{Limit,FEA}$ when modelling with $\delta_{max} = 0$ the prediction of $P_{Limit,FEA}$ is not the highest, which is always predicted with $+\delta_{max}$ (see Table 3), and this finding is shown in Figure 11 using model EC1_1900_TF. This outcome, again, reflects the important influence on buckling strengths from the combination of geometric and material imperfections. The differences in predicted resistances when the boundary conditions are EC2 are for similar ranges, namely: TF_EC2 between 6 and 23% (at 1% lower than EC1 lower and upper bounds); SC_EC2 between 6 and 24% (at 2% lower); BF_EC2 between 6 and 25% (at 2% lower and 3% higher).

To be able to compare ABAQUS® predictions with $P_{Limit,e}$s their differences are expressed, as a percentage, using the formula $\Delta_{Limit} = (P_{Limit,e}/P_{Limit,FEA} - 1)\times100\%$. Note that a positive percentage for Δ_{Limit} means the FE prediction is lower than the experimental test result. Plotted in Figures 12 to 14, for EC1 modelling, is Δ_{Limit} with L (Table 4) for the three loading cases of

TF, SC, and BF. It is noted that there is no single trend on assuming there can be a linear change in Δ_{Limit} between each of the five spans. Inspection does show that at the lower two spans the Δ_{Limit} percentages are mostly positive and at the higher spans they are mostly negative. It is assumed that a difference lying between ±10% is for an acceptable agreement, and so in the figures horizontal lines are introduced to bound the reliable comparisons. There are several data points plotted in Figures 12 to 14 that are within these limits. The physical reason is unknown for why Δ_{Limit} can be > -20% at the largest span of 4048 mm. An explanation could be that there had been an additional imperfection in the testing, from how the vertical load is transferred into the beam [6], that further lowered the measured LTB load.
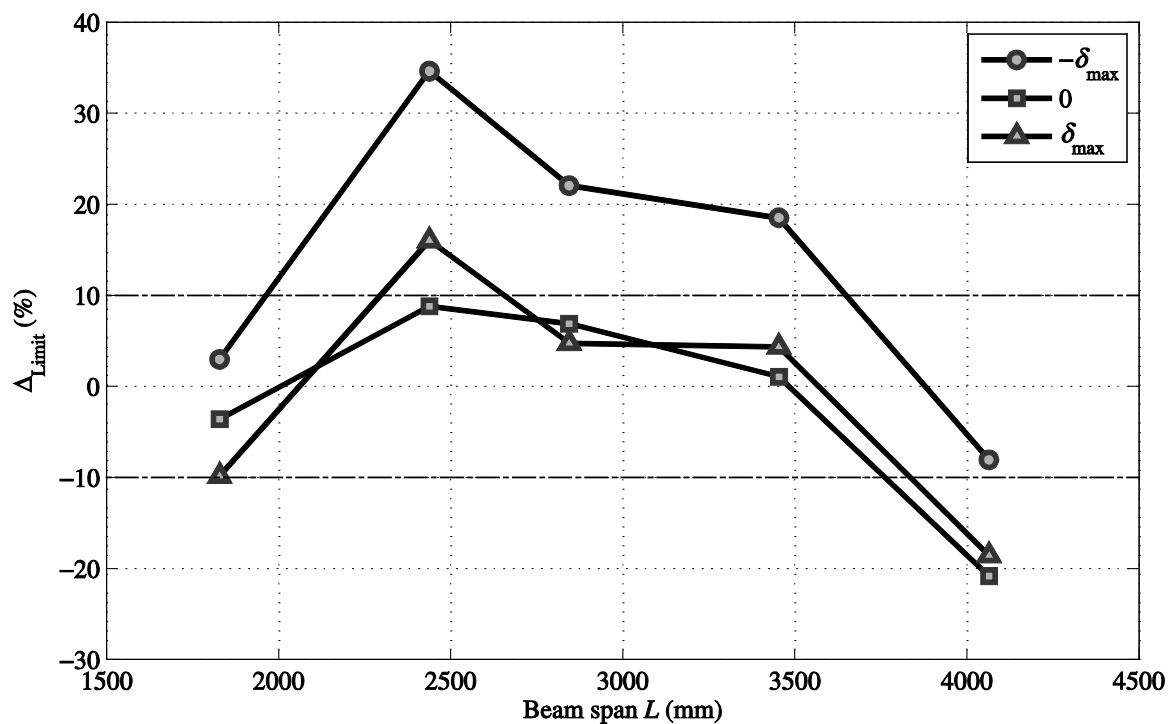

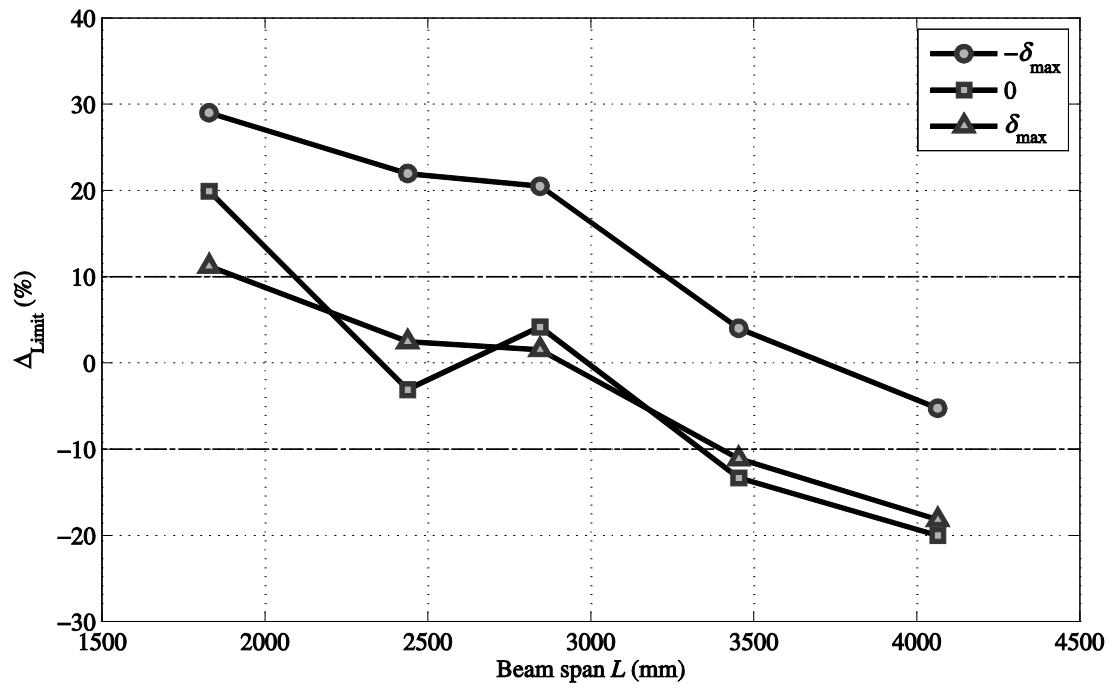Figure 12. Plots of Δ_{Limit} vs. span L for TF_EC1

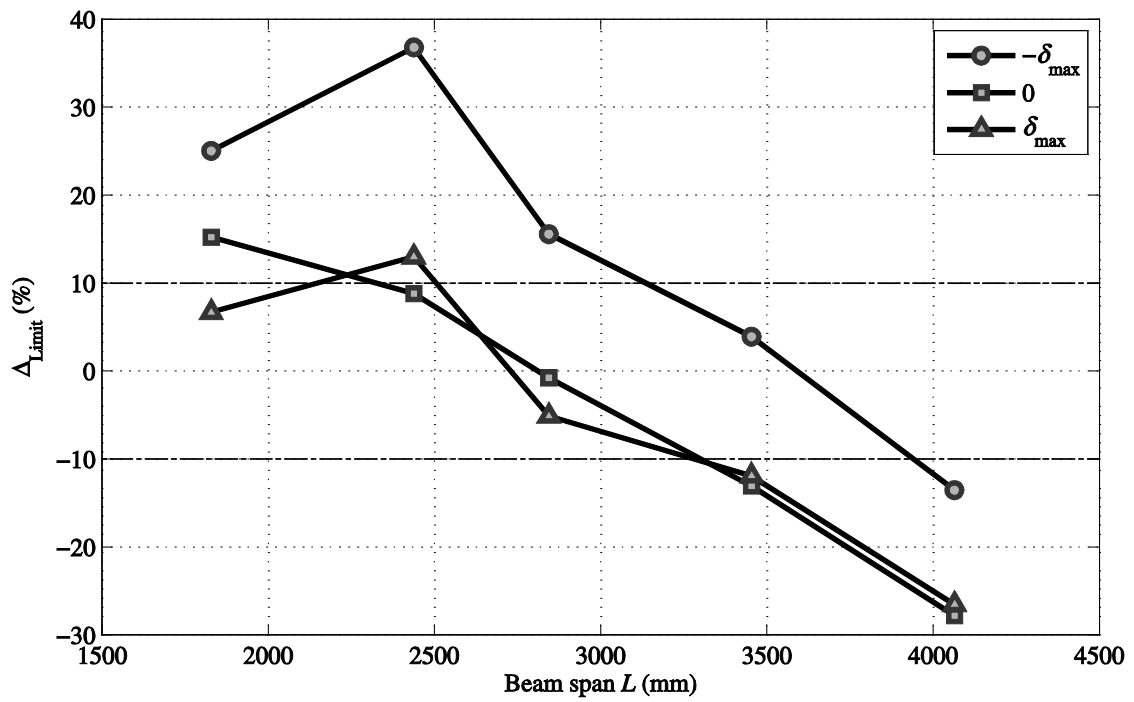Figure 13. Plots of Δ_{Limit} vs. span L for SC_EC1

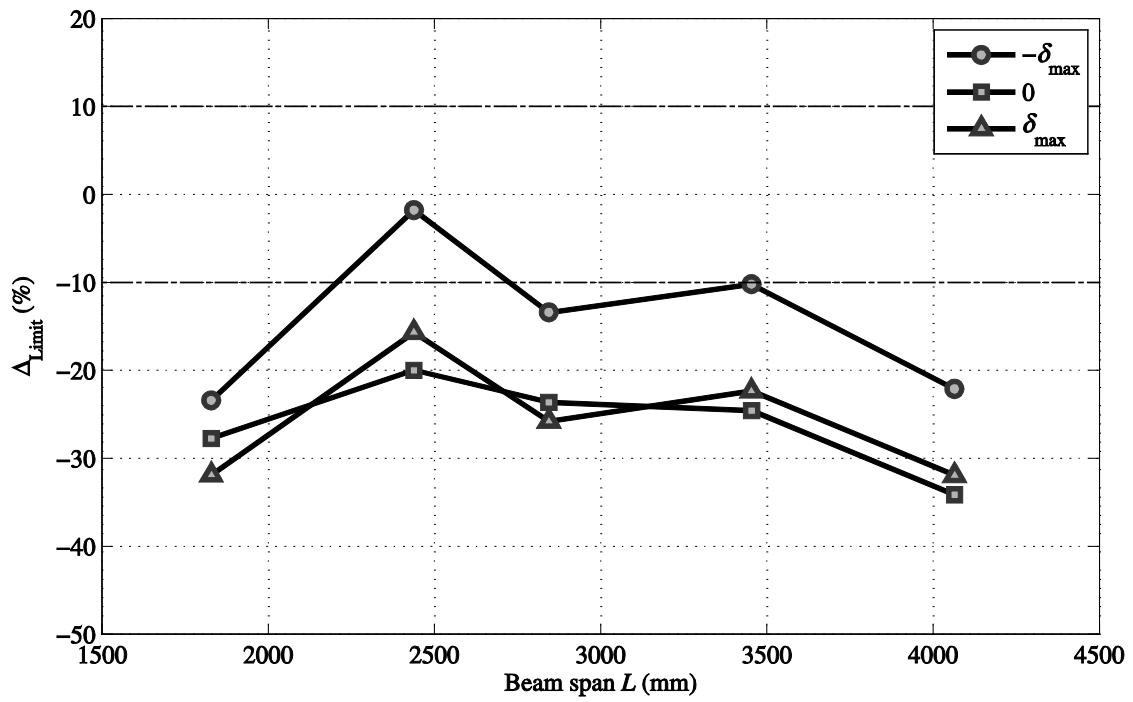Figure 14. Plots of Δ_{Limit} vs. span L for BF_EC1

Figure 15 Plots of Δ_{Limit} vs. span L for TF_EC2
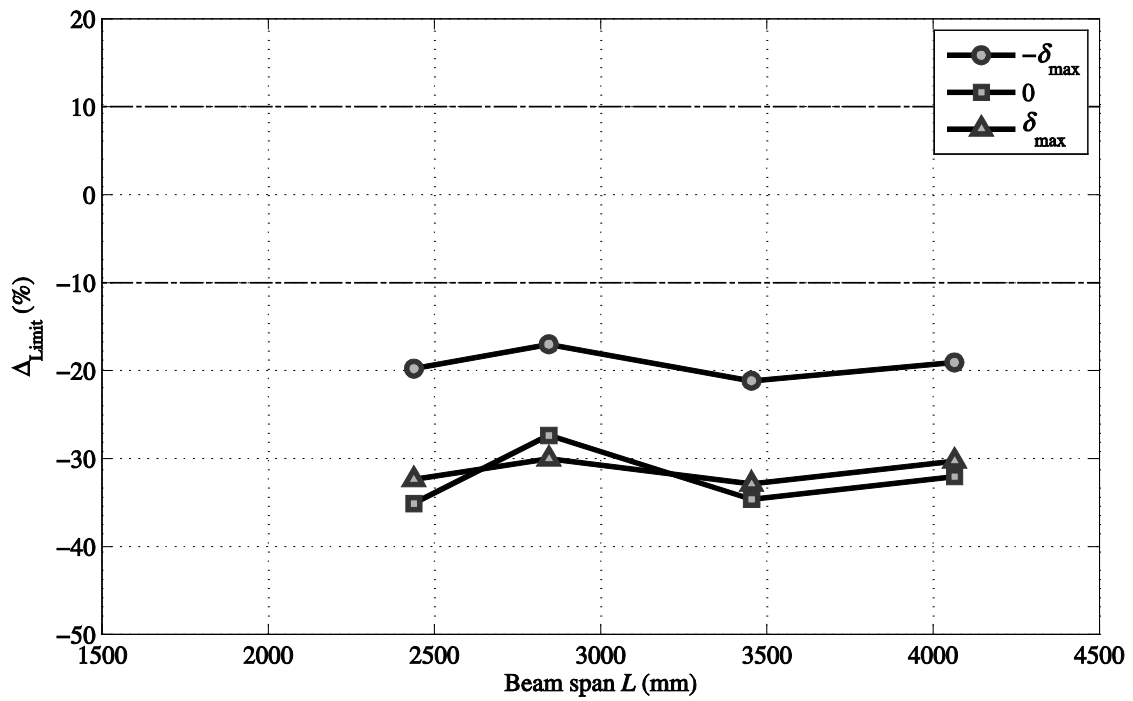

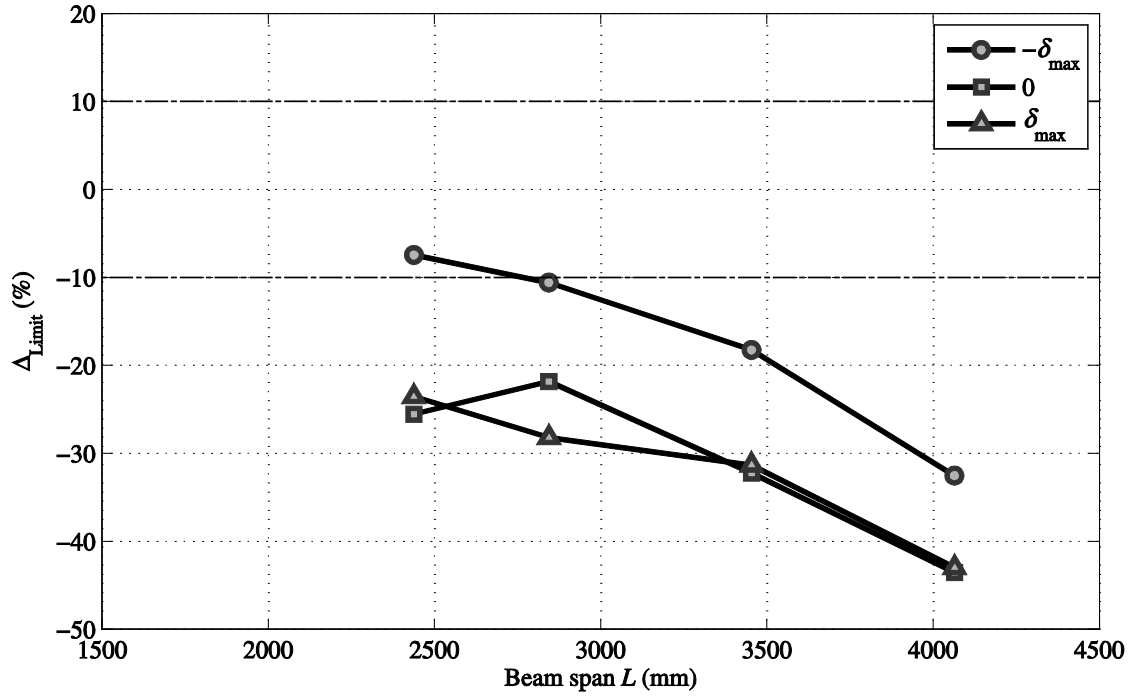Figure 16 Plots of Δ_{Limit} vs. span L for SC_EC2

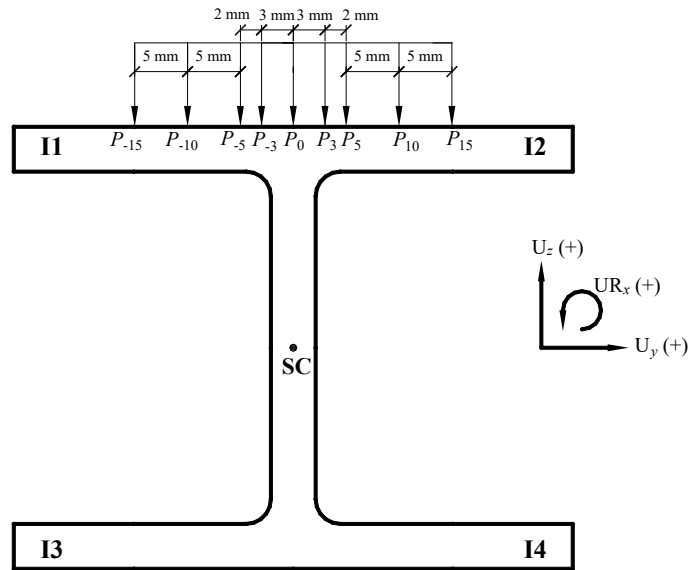Figure 17. Plots of Δ_{Limit} vs. span L for BF_EC2

Figure 18. Lateral load positions for load eccentricities on the top flange (not to scale)

To continue this study, Figures 15 to 17 are the equivalent plots with the FE models having the

EC2 end conditions. Now we observe that for beams where there is end-restraint against lateral

flexure, only three Δ_{Limit}s out of 45 are found to lie within $\pm 10\%$, and the other 42 are for a greater negative percentage, and with the highest being $> 40\%$. Because $P_{\text{Limit,FEA}}$ is $> P_{\text{Limit,e}}$ it can be inferred that the presence of the two steel rods per side per end only gave the beam partial restraint to full fixity against lateral flexure end rotation.

The nonlinear FE predictions to $P_{\text{Limit,FEA}}$ presented in Table 4 and 5 have shown that LTB resistance is sensitive to the magnitude and direction of the initial geometric imperfection (in the form of a minor-axis half-sine wave). Next, a sensitivity study considers the influence of load eccentricity in terms of lateral positioning from the no-eccentricity plane, which is the minor-axis plane passing through the I-section's centroid. Figure 18 illustrates the locations on the top surface of the top flange for nine lateral eccentricities where the vertical load is imposed in FE models. Clearly, the introduction of load eccentricity generates, at the mid-span, a secondary moment or torque that twists the I-beam, with positive rotation in the anti-clockwise direction. The effect of this on reducing the LTB resistance is evaluated by conducting nonlinear FE analyses for the single beam span of 3000 mm, having either EC1 or EC2 end conditions. The modelling methodology also involves a constant initial out-of-straightness imperfection of $\delta_{\text{max}} = -1.95$ mm, as reported for this span in Table 3. The vertical load applied at the vertical plane for the Shear Center (SC) (no-eccentricity case) is denoted as P_0. The other eight positions are offset by 3 mm, 5 mm, 10 mm, and 15 mm from P_0 in both directions and are labelled P_3, P_5, P_{10}, P_{15}, P_{-3}, P_{-5}, P_{-10} and P_{-15}.

Table 5. Limiting buckling loads for FEA (with different δ_{max}) and tests for EC2

| Span (mm)	Top flange $P_{Limit,FEA}$ (kN)			$P_{Limit,e}$ (kN)	Shear center $P_{Limit,FEA}$ (kN)			$P_{Limit,e}$ (kN)	Bottom flange $P_{Limit,FEA}$ (kN)			$P_{Limit,e}$ (kN)
	$-\delta_{max}$	0	$+\delta_{max}$		$-\delta_{max}$	0	$+\delta_{max}$		$-\delta_{max}$	0	$+\delta_{max}$	
1828	8.20	8.69	9.22	6.28	10.7	11.4	12.1	-	15.9	16.8	17.9	-
2438	3.34	4.10	3.89	3.28	4.40	5.44	5.22	3.53	6.17	7.67	7.47	5.71
2844	2.46	2.79	2.87	2.13	3.23	3.69	3.83	2.68	4.44	5.08	5.53	3.97
3454	1.47	1.75	1.70	1.32	1.89	2.28	2.22	1.49	2.52	3.04	3.00	2.06
4064	1.04	1.23	1.19	0.81	1.31	1.56	1.52	1.06	1.69	2.02	2.00	1.14
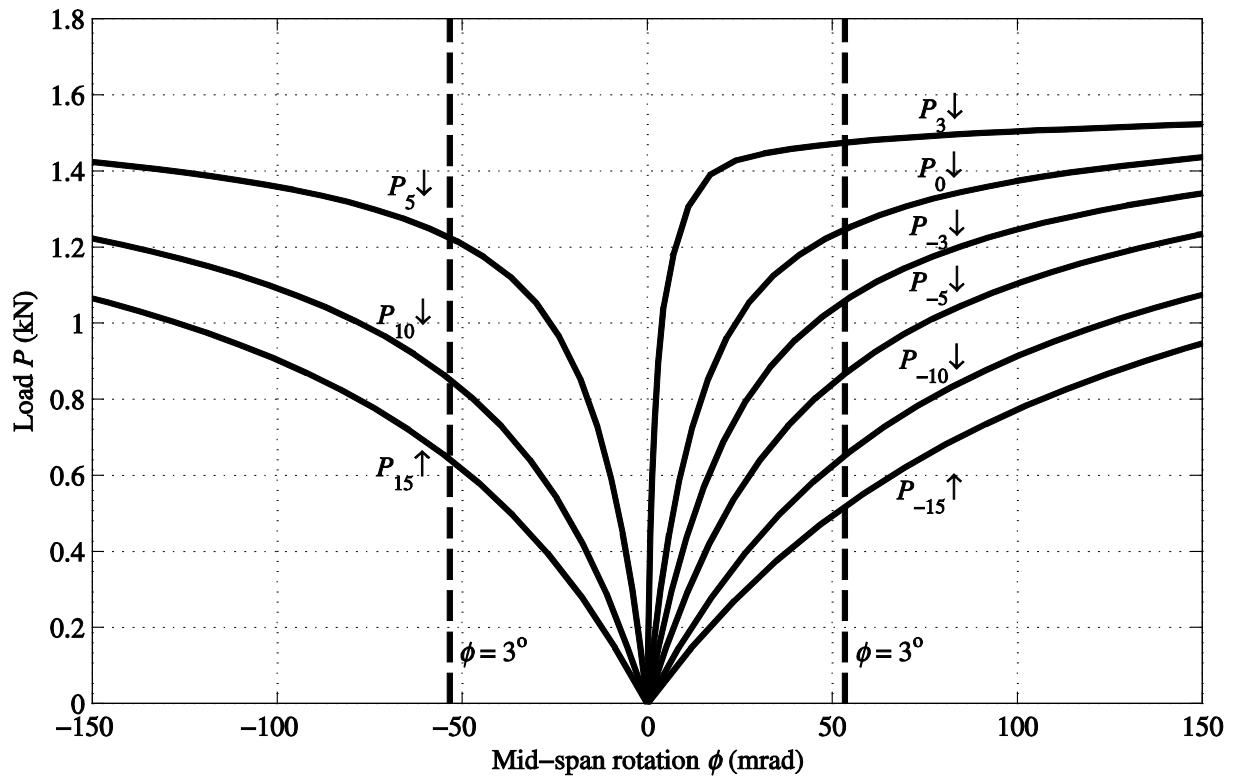
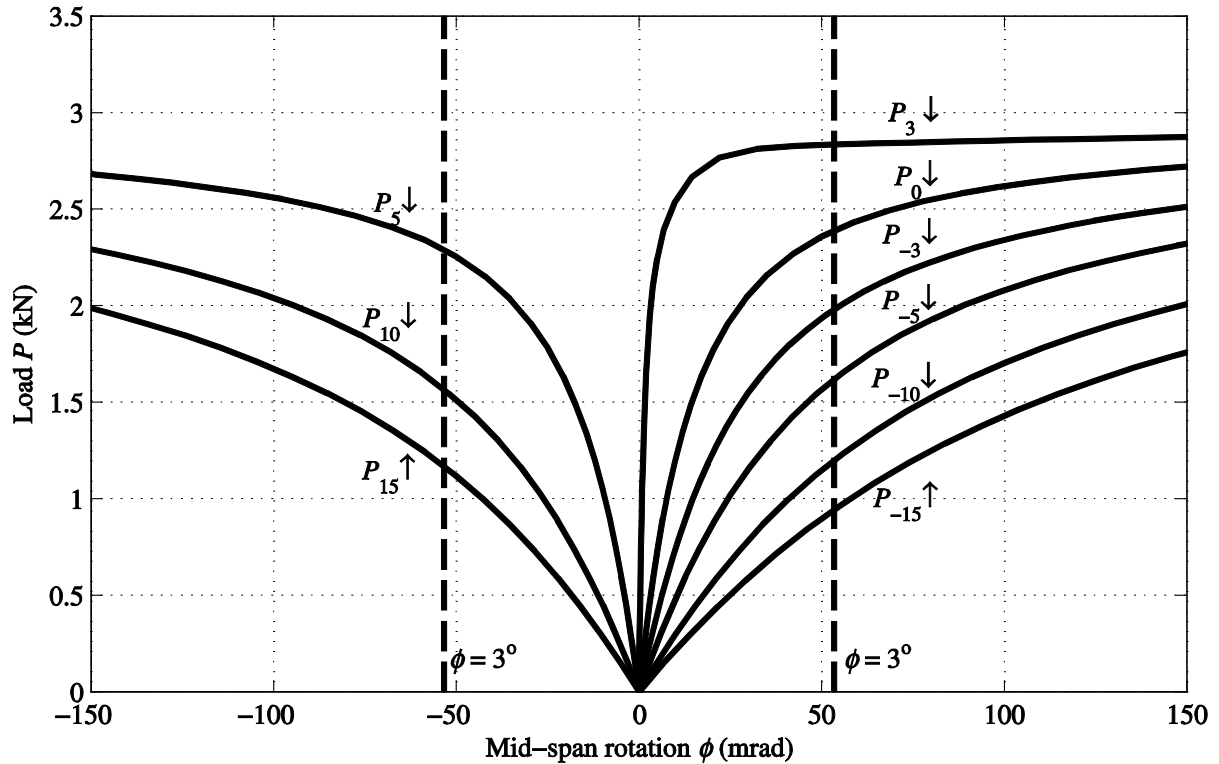Figure 19. P vs. ϕ for EC1_3000_TF for nine lateral load eccentricities (refer to Figure 18)

Figure 20. P vs. ϕ for EC2_3000_TF for nine lateral load eccentricities (refer to Figure 18)

Plotted in Figures 19 and 20 are the predicted P with ϕ curves for nine lateral load eccentricities with end conditions EC1 and EC2, respectively. It is seen in both figures that for the 'no-eccentricity' position P_0 the beam has twist ϕ in the positive direction (i.e., $UR_x > 0$). This twisting is because of the combination in having different elastic constants in the flange outstands I1 to I4 (creating an unsymmetrical beam) and the minor-axis out-of-straightness imperfection (which is on the 'left-side', thereby promoting rotation, ϕ, in the positive direction). Modelling cases with the vertical load having lateral eccentricities on the right-side (i.e., P_{15}, P_{10} and P_5) deform the beam-section at mid-span towards the right with ϕ negative. This shows that the effect on deformation from load eccentricity outweighs the combined effect of the initial geometrical and material imperfections. For load case P_3, that has an eccentricity of 3 mm to the 'right' it is observed that the beam deforms to the 'left', after an initial load

where there is virtually no mid-span rotation. This indicates that the effect of lateral load eccentricity is now opposite and very similar to the combined geometrical and material imperfections. Once load P is applied in the FE analyses for the five load eccentricities of P_0, P_{-3}, P_{-5}, P_{-10} and P_{-15} there is rotation from beam twisting that is positive (to the 'left').
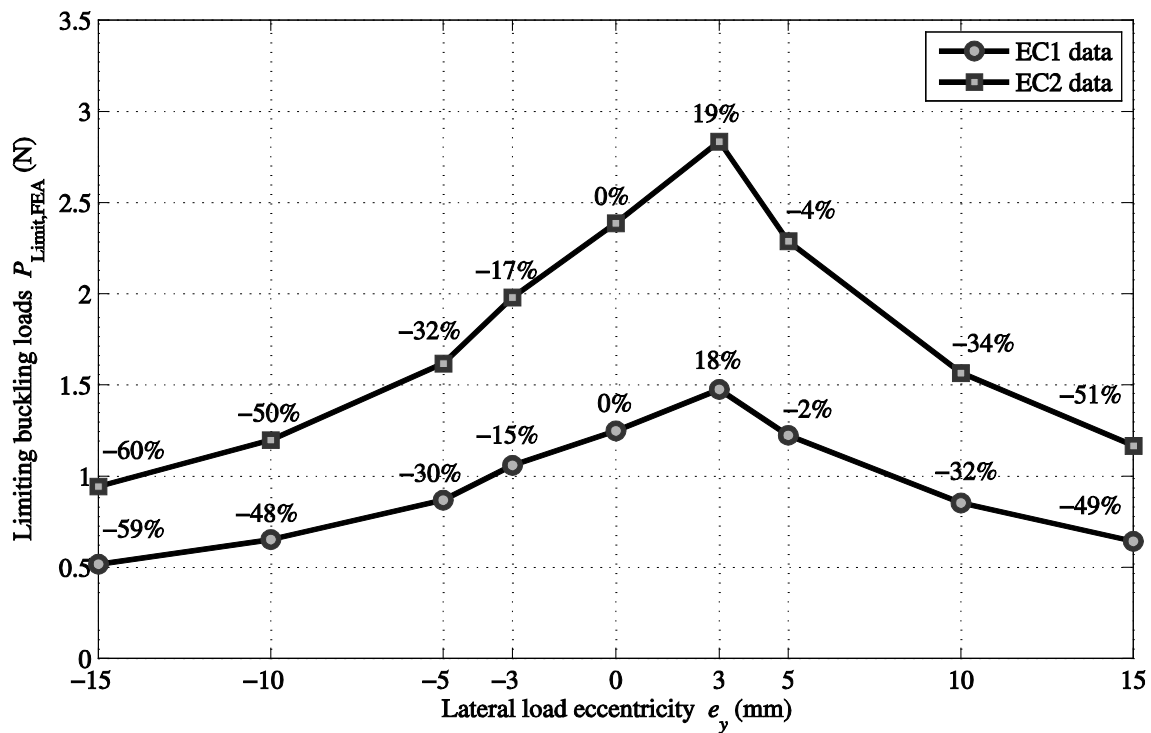

Figure 21. Influence of lateral load eccentricity (e_y) on $P_{\text{Limit,FEA}}$ for beams EC1_3000_TF and EC2_3000_TF

Plotted in Figure 21 are the $P_{\text{Limit,FEA}}$s obtained when $\phi = 3°$ with increasing lateral load eccentricity, e_y. For end conditions EC1, the nine plotted values are with a circular symbol and when displacement boundary conditions are changed to EC2 the equivalent nine data points are with a square symbol. The points have been connected for a linear trend curve. The results, as presented in Figure 21, show that $P_{\text{Limit,FEA}}$ is highest for load case P_3. Whilst the limiting buckling load for P_3 is 19% higher than for P_0, $P_{\text{Limit,FEA}}$ with P_{-3} is 15% lower. One important finding from this sensitivity study is to observe that from the shapes of the two curves in Figure 21 the variation in $P_{\text{Limit,FEA}}$ with e_y is not influenced by end conditions of EC1 or EC2.

4. CONCLUDING REMARKS

Presented is the modeling methodology using ABAQUS® Finite Element (FE) package to conduct sensitivity analyses for the Lateral Torsional Buckling (LTB) instability of flexural members of Pultruded Fibre Reinforced Polymer (PFRP). The thin-walled panels in the flange outstands and web of the single I-section are treated as single-layered transverse isotropic materials, but with different elastic constants, which introduces a constant material imperfection. The PFRP profile is of size 120x60x6 mm, and the spans modelled are from 1500 to 4046 mm. The loading arrangement is for three-point bending. Adopted element type following a study on the numerical performance of various shell elements in the ABAQUS® element library is the 8-noded thick shell element (S8R) with side length of maximum 15 mm along the beam's mesh. The fillet volumes at the flange-web junctions are modelled by assigning 'increased constant thickness' elements in these four specific localized regions. The modelling and simulation parameters varied in the sensitivity studies are: vertical loading positions; lateral loading eccentricity; end boundary conditions at the simple supports; geometrical imperfections. The FE results for LTB resistances were validated against relevant and reliable physical test results taken from the PhD thesis of the first author. The following observation and findings can be drawn from this new contribution:

1. The FE modelling methodology that includes the additional fillet radius volumes gives considerably better comparison for predicted LTB resistances with respect to the experimental limiting buckling loads.

2. It is found that the influence on LTB resistance of the vertical load height (relative to the shear center of the I-section) is very significant when the material is PFRP. It has been shown that, when compared to shear centre loading, the numerical limiting buckling load can decrease by 20% for top flange loading and increase by 30% for bottom flange loading. In other words, the reported sensitivity study is for a 50% difference in LTB resistance

between the load introduced at the top or bottom flange, and without any lateral load eccentricity.

3. As expected, a flexural member's deformation response and resistance is significantly influenced by the lateral position of the vertical loading. This FE sensitivity study shows that, for the specific geometrical and material imperfections modelled, having a load eccentricity of 3 mm predicts a limiting buckling load that will either be reduced by up to 17% or increased by up to 19%. This significant change in resistance is dependent on how the secondary moment from the presence of the load eccentricity is interacting with the combination of the initial geometrical and material imperfections.

Further sensitivity studies with other FE modelling and simulation parameters are required to be able to fully understand the quantified overall influences from practical combinations of geometrical and material imperfections, eccentric lateral loads, and vertical loading positions.

References

[1]. Mottram, J.T. and Henderson. J. (Eds), *FRP Bridges – Guidance for Designers*, prepared by Composites UK: Construction Sector Group, CIRIA C779, London, 2018.

[2]. Mottram, J.T., Lateral-torsional buckling of a pultruded I-beam. *Composites*, 23(2), 1992, p. 81-92.

[3]. Ascione, F. and Mancusi, G., The influence of the web-flange junction stiffness on the mechanical behaviour of thin-walled pultruded beams. *Composites Part B: Engineering*, 55, 2013, pp.599-606.

[4]. Ascione, F., Influence of initial geometric imperfections in the lateral buckling problem of thin walled pultruded GFRP I-profiles. *Composite Structures*, 112, 2014, pp.85-99.

[5]. Stoddard, W.P., *Lateral-torsional Buckling Behavior of Polymer Composite I-Shaped Members*, 1997, Ph.D. Thesis. Georgia Institute of Technology: Georgia, USA.

[6]. Nguyen, T.T., *Lateral-Torsional Buckling Resistance of Pultruded Fibre Reinforced Polymer Shapes*, 2014, Ph.D. Thesis. The University of Warwick, UK.

[7]. Feo, L., Mosallam, A.S. and Penna, R., Mechanical behavior of web–flange junctions of thin-walled pultruded I-profiles: An experimental and numerical evaluation. *Composites Part B: Engineering*, 48, 2013, pp.18-39.

[8]. Mancusi, G., Ascione, F. and Lamberti, M., Pre-buckling behavior of composite beams: A mechanical innovative approach. *Composite Structures*, 117, 2014, pp.396-410.

[9]. Quadrino, A., Penna, R., Feo, L. and Nisticò, N., Mechanical characterization of pultruded elements: Fiber orientation influence vs web-flange junction local problem. Experimental and numerical tests. *Composites Part B: Engineering*, 142, 2018, pp.68-84.

[10]. Mosallam, A.S., Feo, L., Elsadek, A., Pul, S.E.L.İ.M. and Penna, R., Structural evaluation of axial and rotational flexibility and strength of web–flange junctions of open-web pultruded composites. *Composites Part B: Engineering*, 66, 2014, pp.311-327.

[11]. Feo, L., Mosallam, A.S. and Penna, R., Mechanical behavior of web–flange junctions of thin-walled pultruded I-profiles: an experimental and numerical evaluation. *Composites Part B: Engineering*, 48, 2013, pp.18-39.

[12]. Kollár, L.P., Local buckling of fiber reinforced plastic composite structural members with open and closed cross sections. *Journal of Structural Engineering*, 129(11), 2003, pp.1503-1513.

[13]. Barbero, E.J. and Raftoyiannis, I.G., Local buckling of FRP beams and columns. *Journal of Materials in Civil Engineering*, 5(3), 1993, pp.339-355.

[14]. Tomblin, J. and Barbero, E., Local buckling experiments on FRP columns. *Thin-Walled Structures*, 18(2), 1994, pp.97-116.

[15]. Silvestre, N. and Camotim, D., GBT buckling analysis of pultruded FRP-lipped channel members. *Computers and Structures*, 81(18-19), 2003, pp.1889-1904.

[16]. Barbero, E. and Tomblin, J., A phenomenological design equation for FRP columns with the interaction between local and global buckling. *Thin-Walled Structures*, 18(2), 1994, pp.117-131.

[17]. Liu, T., Vieira, J.D. and Harries, K.A., Lateral torsional buckling and section distortion of pultruded GFRP I-sections subject to flexure. *Composite Structures*, 225, 2019, Article number 111151.

[18]. Nguyen, T.T., Chan, T.M. and Mottram, J.T., Lateral–Torsional Buckling design for pultruded FRP beams. *Composite Structures*, 133, 2015, pp.782-793.

[19]. Fascetti, A., Feo, L. and Abbaszadeh, H., A critical review of numerical methods for the simulation of pultruded fiber-reinforced structural elements. *Composite Structures*, 273, 2021, p.114284.

[20]. Jones R.M. *Mechanics of Composite Materials*. Philadelphia: Taylor & Francis; 1999.

[21]. Tsai, S.W. *Strength Characteristics of Composite Materials*. Philco Corp Newport Beach CA, 1965.

[22]. Barbero, E. J., Cosso, F. A., Roman, R. and Weadon, T. L., Determination of material parameters for Abaqus progressive damage analysis of E-glass epoxy laminates. *Composites Part B: Engineering*, 46, 2013, 211–220.

[23]. Hashin, Z., Failure criteria for unidirectional fiber composites. *Journal of Applied Mechanics*, 47(2), 1980, 329–334.

[24]. Hashin, Z., and Rotem, A., A fatigue failure criterion for fiber reinforced materials. *Journal of Composite Materials*, 7(4), 1973, 448–464.

[25]. Silva, N.M.F., Camotim, D., Silvestre, N., Correia, J.R. and Branco, F.A., First-order, buckling and post-buckling behaviour of GFRP pultruded beams. Part 2: Numerical simulation. *Computers and Structures*, 89(21-22), 2011, pp.2065-2078.

[26]. Fernandes, L.A., Nunes, F., Silvestre, N., Correia, J.R. and Gonilha, J., Web-crippling of GFRP pultruded profiles. Part 2: Numerical analysis and design. *Composite Structures*, 120, 2015, pp.578-590.

[27]. Nunes, F., Correia, J.R. and Silvestre, N., Structural behavior of hybrid FRP pultruded beams: Experimental, numerical and analytical studies. *Thin-Walled Structures*, 106, 2016, pp.201-217.

[28]. Nunes, F., Silvestre, N. and Correia, J.R.,. Structural behaviour of hybrid FRP pultruded columns. Part 2: Numerical study. *Composite Structures*, 139, 2016, pp.304-319.

[29]. Dassault Systèmes Simulia Corp, *ABAQUS/Standard Ver 6.13*, 2013: Providence, RI, USA.

[30]. Correia, J.R., Branco, F.A., Silva, N.M.F., Camotim, D. and Silvestre, N., First-order, buckling and post-buckling behaviour of GFRP pultruded beams. Part 1: Experimental study. *Computers and Structures*, 89(21–22), 2011, p. 2052-2064.

[31]. Nguyen, T.T., T.M. Chan and J.T. Mottram, Lateral-torsional buckling resistance by testing for pultruded FRP beams under different loading and displacement boundary conditions. *Composites Part B: Engineering*, 60, 2014, p. 306-318.

[32]. Hyer, M.W. and S.R. White, *Stress Analysis of Fiber-Reinforced Composite Materials*. 1998, Singapore: WCB/Mc Graw-Hill.

[33]. Tuttle, M.E., *Structural Analysis of Polymeric Composite Materials*. 2012, CRC Press.

[34].   Dassault Systèmes Simulia Corp, *Theory Manual*, ver 6.13, 2013: Providence, RI, USA.

[35].   Brooks, R.J. and G.J. Turvey, Lateral buckling of pultruded GRP I-section cantilevers. *Composite Structures*, 32(1–4), 1995, p. 203-215.

[36].   Turvey, G.J., Effects of load position on the lateral buckling response of pultruded GRP cantilevers - Comparisons between theory and experiment. *Composite Structures*, **35**(1), 1996, p. 33-47.

[37].   Qiao, P.Z., Zou, G.P. and Davalos, J.F., Flexural–torsional buckling of fiber-reinforced plastic composite cantilever I-beams. *Composite Structures*, 60(2), 2003, p. 205-217.

[38].   Shan, L.Y. and Qiao, P.Z., Flexural–torsional buckling of fiber-reinforced plastic composite open channel beams. *Composite Structures*, 68(2), 2005, p. 211-224.

[39].   Mottram, J.T. and Shaw, C.T., *Using Finite Elements in Mechanical Design*. 1996, London: McGraw Hill.

[40].   Kollár, L.P. and Springer, G.S., *Mechanics of Composite Structures*. 2003, Cambridge: University press.

[41].   Sapkás, A. and Kollár, L.P., Lateral-torsional buckling of composite beams. *International Journal of Solids and Structures*, 39(11), 2002, p. 2939-2963.

[42].   BS EN 13706-2:2002, *Reinforced Plastic Composites - Specifications for Pultruded Profiles - Part 2: Method of Test and General Requirements*, British Standards Institution: London, UK.

[43].   Bureau, A., *NCCI: Elastic critical moment for lateral-torsional buckling*. SN003a-ENEU. Access Steel, 2006.

[44].   Trumpf, H., *Local and Global Stability of Plane Frame Works Made of Orthotropic FRP Profiles*, 2006, University of Aachen, Germany: Shaker-Verlag.

[45]. Schleich, J.B., Chantrain, P., Chabrolin, B., Galéa, Y., Bureau, A., Anza, J. and Espiga, F., *Promotion of Plastic Design for Steel and Composite Cross-Sections: New Required Conditions in Eurocodes 3 and 4, Practical Tools for Designers*, Final Report, EUR 18366, Luxembourg, 1998.

[46]. Dassault Systèmes Simulia Corp, *Abaqus Analysis User's Guide*, ver. 6.13, 2013: Providence, RI, USA.

[47]. Riks, E., An incremental approach to the solution of snapping and buckling problems. *International Journal of Solids and Structures*, 15(7), 1979, p. 529-551.

[48]. Crisfield, M.A., A fast incremental/iterative solution procedure that handles "snap-through". *Computers and Structures*, 13(1), 1981, p. 55-62.

[49]. Lee, S., *Flexural-Torsional Buckling of Pultruded T-sections*, Ph.D. Thesis, 2003, Georgia Institute of Technology: Georgia, USA.

[50]. Nguyen, T.T., T.M. Chan, and Mottram, J.T., Influence of boundary conditions and geometric imperfections on lateral–torsional buckling resistance of a pultruded FRP I-beam by FEA. *Composite Structures*, 100(0), 2013, p. 233-242.

Nomenclature used in this paper

e_y - Lateral load eccentricity from the minor-axis centroid plane of the cross-section (mm)

b - Breadth of I-section (mm)

h - Depth of I-section (mm)

k - Restraint factor for lateral flexural bending at end supports; 0.5 for full restraint to 1.0 for fully unrestrained

k_w - Restraint factor for warping at end supports; 0.5 for full restraint to 1.0 for fully unrestrained

x - Distance along the length of a beam (mm)

w	-	Vertical deflection at mid-span (mm)
E_L	-	Longitudinal modulus of elasticity (tensile), E_1 (GPa)
E_T	-	Transverse modulus of elasticity (tensile), E_2 (GPa)
G_{LT}	-	In-plane shear modulus, G_{12} or G_{13} (GPa)
G_{TL}	-	Out-of-plane shear modulus, G_{23} (GPa)
v_{LT}	-	Major Poisson's ratio
I_T	-	Torsional constant (mm^4)
I_w	-	Warping rigidity (mm^6)
I_y	-	Second moment of area for flexure about the beam's major-axis (mm^4)
I_z	-	Second moment of area for flexure about the beam's minor-axis (mm^4)
L	-	Major-axis flexural span of beam for defining the magnitude of out-of-straightness (mm)
L_b	-	Lateral unrestrained span (mm)
P	-	Central vertical point load which can be applied at different heights from the shear centre of the I-section (kN)
P_{cr}	-	Elastic critical buckling load for lateral-torsional failure of a simply supported beam subjected to central point loading (kN)
$P_{cr,sh}$	-	Elastic critical buckling load for lateral-torsional failure with shear deformation of a simply supported beam subjected to central point loading (kN)
$P_{cr,FEA}$	-	Elastic critical buckling load obtained from linear (Eigenvalue) finite element analysis (kN)
$P_{Limit,FEA}$	-	Limit load for lateral-torsional buckling failure by Finite Element Analysis (kN)
$P_{Limit,e}$	-	Limit load for lateral-torsional buckling failure by experiment (kN)
z_g	-	Distance (height) from the shear centre to the point of load application (mm)
δ_{max}	-	Maximum out-of-straightness imperfection at mid-span (mm)
ϕ	-	Mid-span rotation (rad)